Interpretation of the Al K- and $L_{II/III}$-edges of aluminium oxides: differences between tetrahedral and octahedral Al explained by different local symmetries

2001 J. Phys.: Condens. Matter 13 10247

(http://iopscience.iop.org/0953-8984/13/45/311)

INSTITUTE OF PHYSICS PUBLISHING JOURNAL OF PHYSICS: CONDENSED MATTER

J. Phys.: Condens. Matter **13** (2001) 10247–10260 PII: S0953-8984(01)24741-9

Interpretation of the Al K- and $L_{II/III}$-edges of aluminium oxides: differences between tetrahedral and octahedral Al explained by different local symmetries

J A van Bokhoven[1,2], T Nabi[1], H Sambe[1], D E Ramaker[1] and D C Koningsberger[2]

[1] Chemistry Department, George Washington University, Washington, DC 20052, USA
[2] Department of Inorganic Chemistry and Catalysis, Debye Institute, Utrecht University, Sorbonnelaan 16, 3584 CH Utrecht, The Netherlands

E-mail: J.A.vanBokhoven@chem.uu.nl

Received 10 May 2001, in final form 16 August 2001
Published 26 October 2001
Online at stacks.iop.org/JPhysCM/13/10247

Abstract

The Al K- and $L_{II/III}$-edge XANES of aluminium oxide are interpreted using empirical molecular orbital theory (EHMO) and *ab initio* self-consistent field real space multiple scattering calculations (FEFF8). Most features in the XANES at the K- and $L_{II/III}$-edges are interpreted as shape resonances; although some fine structure, visible at both edges, arises from multiple scattering over the medium range (∼15 Å). The change in local symmetry between octahedral and tetrahedral Al explains the observed differences in the electronic structure. First, Al p–d hybridization is allowed only in tetrahedral symmetry, resulting in a lower absorption edge in tetrahedral Al than in the octahedral. Second, only in octahedral Al do the oxygen orbitals near the valence band maximum (the HOMOs) have the right symmetry to mix with the Al p orbitals just above the band gap (the LUMOs). This gives a more screened core hole in the octahedral case. Calculations on *distorted* octahedral Al sites reveal both p–d and s–d hybridizations; however, the latter is less prominent. The diffuse d orbitals, which hybridize with the p or s orbitals in tetrahedral or distorted octahedral symmetry, are primarily responsible for the fine structure in the near-edge region (0–15 eV) that is determined by medium-range scattering (up to ∼15 Å). The observed difference in the magnitude of this fine structure at the K- and $L_{II/III}$-edges is caused by the different degrees of d orbital hybridization with the s and p orbitals.

1. Introduction

Recently, we showed that Al K-edge spectra are a useful source for obtaining structural information on Al-containing compounds [1]. Characteristic features in each spectrum enable a 'fingerprint' of Al in different coordinations. Several other papers have described a similar fingerprinting technique [2–8]. In contrast, other recent papers have set out to interpret the spectra based on full [9] or partial [10] multiple scattering calculations, or on MO calculations [11]. Using these calculations, a reasonable insight into the origin of these characteristic features in the spectra is obtained. The multiple scattering (MS) methods are especially able to reproduce the experimental spectra. However, a specific question concerning the nature of the core hole screening in the XANES final state surfaced from these calculations. This question must be answered before one can understand the changes seen upon the adsorption of aromatic hydrocarbons on the surface of pores in zeolites [12, 13]. The adsorption of the aromatic hydrocarbons on tetrahedral Al in zeolite beta changes the K-edge spectra dramatically when measured in the electron yield mode. The Al XAS initially exhibit the characteristic features of the tetrahedral Al as expected, but upon adsorption of the aromatic hydrocarbons exhibit several characteristic features of octahedral Al, even though it is known that the geometry of the tetrahedral Al framework does not significantly alter by the chemisorption.

Cabaret *et al* [9] succeeded in reproducing the Al K-edge spectra of tetrahedral and octahedral Al in crystalline compounds by performing multiple scattering calculations using the 'extended continuum' code [14]. A relation between the structural parameters and the spectral features was obtained. Moreover, from their calculations, the electronic structures of the compounds were determined. They found that in the tetrahedral case an unscreened potential had to be used in order to reproduce the spectra, whereas for the octahedral compounds, a screened potential was used. Based on density of states (DOS) calculations on SiO_2 [15] and corundum [16], it was concluded that the reason for this difference was that the DOS near the valence band maximum (VBM) in tetrahedral Al is anion-like with a strong p character, whereas in the distorted octahedral case the VBM contains a higher cation DOS. As a result, the core hole screening, most effectively done by the electrons at the VBM, will be less complete in the tetrahedral case. So, the question that is addressed here is, why do these differences in electronic structure near the VBM in the tetrahedral and octahedral Al symmetries appear?

A second question concerns the nature of the fine structure in the 0–15 eV range of the K- and $L_{II/III}$-edge spectra: why is the structure in this range so dependent on long-range MS and why is this structure more dominant in the K-edge than in the $L_{II/III}$-edge? Cabaret *et al* [9] and others [10] have found that the clusters up to 15 Å are required to fully reproduce the fine structure in this region. This fine structure, if fully understood, could be utilized as a fingerprint for the presence of crystalline versus amorphous Al [17], or even as a measure of cluster size in various catalysts [1].

Here we show that these differences between the electronic structures of octahedral and tetrahedral Al can be understood simply from the different local symmetries. Two primary differences are evident: (1) a different level of hybridization (a term used here for a linear combination of *atomic* orbitals) of the p and d orbitals for different coordinations and (2) a different level of mixing (a term used here for a linear combination of *molecular* orbitals) of the oxygen orbitals near the VBM with Al; this mixing facilitates the screening of the core hole. Using the extended Hückel molecular orbital (EHMO) method, the influence of hybridization on the spectra is examined. The EHMO includes a full treatment of the local symmetry and therefore it is suitable for investigating the simple hybridization of the orbitals in different coordinations, although it is known to provide only qualitative results

because of the many approximations. While the orbital hybridization is determined by EHMO calculations, full real-space multiple scattering (FMS), self-consistent field (SCF) calculations have been performed using FEFF8. Moreover, using this code, the DOS can be calculated. These DOS are compared to the experimental data and the EHMO calculations.

We further show that the same p–d and s–d hybridizations and the diffuse nature of the d orbitals explain the reason for the long-range MS structure and the differences in the magnitude of this phenomenon in the K- and $L_{II/III}$-edges.

2. Methods

To obtain an insight into the origin of the features in the spectra and the role of orbital symmetry, we performed semi-empirical molecular orbital calculations using the EHMO code [18] with the parameters provided by Burns [19]. This allows a choice of including or omitting the d orbitals in the calculations. The EHMO calculations give as output (among others) the energy and atomic orbital content of the localized shape resonances that are used to interpret the XANES data. The relative XANES intensities are determined by the molecular orbital coefficients of s/d character at the $L_{II/III}$-edge and p character at the K-edge on the absorber atom. The EHMO method gives the qualitative trends satisfactorily; however, particularly in the strong anti-bonding region, the energies from EHMO are quantitatively not correct. Nevertheless, the nature of the orbital hybridization (defined as occurring intra-atomic) and mixing (inter-atomic) can be studied using the EHMO.

The inputs required for this code are the geometrical coordinates and the electronic charge on the cluster. We want filled MOs in the calculations, which require relatively large electronic charges on the clusters. In order to account for the core hole in the final state of the x-ray absorption transition, which is reflected in the XANES data, the Z + 1 rule [20] was utilized; i.e. the absorbing atom was assumed to be a Si atom mimicking the final-state core hole. We call this atom $Al^{\underline{c}}$; thus $Al^{\underline{c}}O_x^{-y}$ clusters were used. For tetrahedral and octahedral Al coordinations $Al^{\underline{c}}O_4^{-5}$ and $Al^{\underline{c}}O_6^{-8}$, respectively, are used. Various clusters with different Al–O bond lengths and distortions from ideal O_h symmetry were utilized.

A shape resonance can be visualized as a multiple scattering wave in the first coordination sphere that is condensed by higher order resonance. Therefore, the XANES spectra can be reproduced by multiple scattering calculations, such as those performed in the FEFF code, which employs self-consistent real-space multiple scattering cluster calculations [21–23]. Details have been published elsewhere [1]. The output of the FEFF8 calculations are (among others) the XAS spectral lineshapes and the DOS. Calculations are performed on increasingly larger clusters, with a maximum diameter of $\sim$18 Å.

The potential used in the FEFF8 calculations is the Hedin Lundqvist potential, as using this potential the best agreement with the experiment was obtained.

The experimental spectra that are shown in this study are aligned at the bottom of the conduction band as estimated from the spectra.

3. Results

3.1. Parameters determining Al XAS

In order to summarize the factors influencing the shape of the Al XAS spectra, an Al K-edge spectrum for tetrahedrally coordinated aluminium oxide is built up step by step, and shown schematically in figure 1. Throughout the text, the dominating factors that determine the final

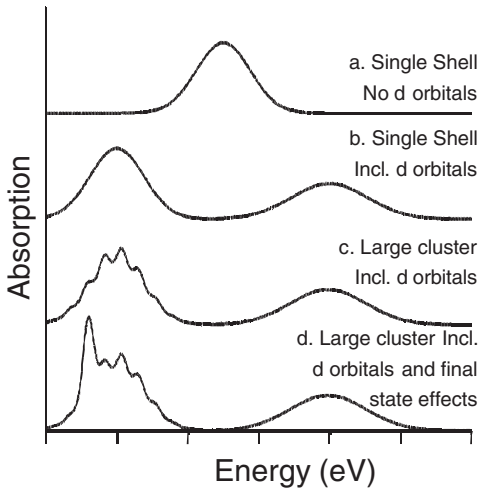

Figure 1. Schematic representation of an Al K-edge spectrum for aluminium oxide with an Al in a tetrahedral site, based on molecular orbital and multiple scattering calculations (this figure is discussed throughout the text). The expected spectra for: (a) an Al atom surrounded by only one shell of O atoms without the participation of the Al d orbitals, (b) one O shell with the participation of the Al d orbitals, (c) a large cluster ($D > 30$ Å) including d orbitals and (d) a large cluster including d orbitals and in the presence of a core hole, which reproduces the experimental spectra.

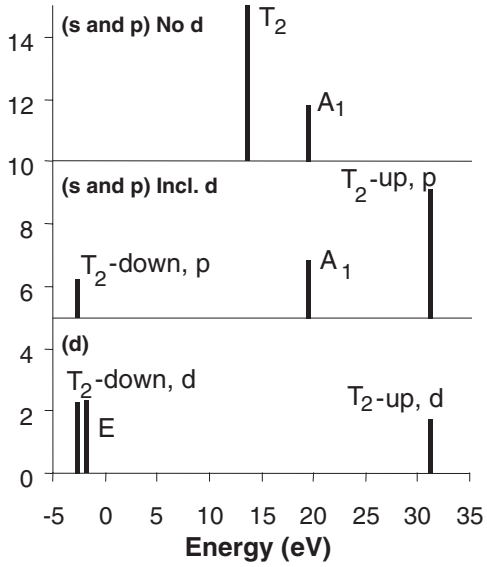

Figure 2. Results of EHMO calculations on an $Al^{c}O_4^{5-}$ cluster with Al in T_d symmetry. The top section shows the results without the inclusion of the Al d orbitals. The middle (s and p orbital content) and bottom (d orbital content) sections show the results after the inclusion of the Al d orbitals and the effects of strong p–d hybridization.

shape of the edge are discussed, such as p–d hybridization, HOMO/LUMO mixing, long-range MS, screening effects and bond length sensitivity. The figure is based on molecular orbital and full multiple scattering calculations, partly taken from the literature. The differences and similarities between the tetrahedral and octahedral coordinated aluminium oxides are discussed.

3.2. Orbital hybridization in tetrahedral Al

Figure 2 shows the results of the EHMO calculations on a tetrahedral Al cluster, $Al^{c}O_4^{-5}$, with an Al–O bond length of 1.70 Å. At the top, the unoccupied s- and p-DOS are shown as calculated without the inclusion of the d orbitals in the calculation. An A_{1g} and a T_2 level, with s and p characters respectively, are found. Inclusion of the d orbitals into the EHMO calculation dramatically changes the picture. Whereas the A_{1g} level is not affected, the T_2 level is divided into two energy levels, which we call T_2-up and T_2-down, reflecting their relative position with respect to the original T_2 level. The T_2-up/down levels have both p and d characters resulting from p–d hybridization, which is allowed in a tetrahedral conformation. However, no d–s hybridization is allowed. Moreover, an additional energy level of E_g symmetry having solely d character appears. This splitting of the d orbitals into a T_2 and an E_g level is expected from the crystal field theory in a tetrahedral conformation.

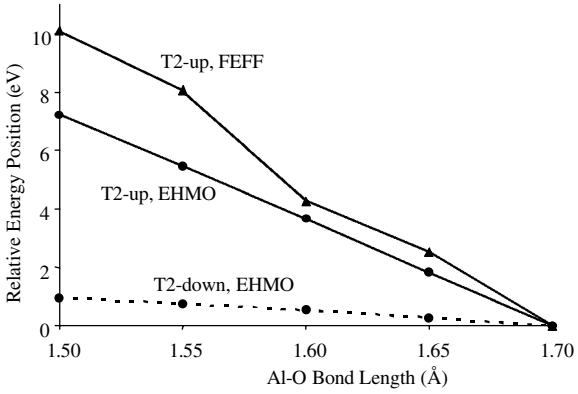

Figure 3. Evolution of the relative energies of the T_2-up and T_2-down levels as a function of the Al–O bond length as determined from the EHMO and FEFF calculations. The energy values are set equal to zero at the Al–O bond length = 1.70 Å for ease of comparison. The T_2-up is strongly Al–O-dependent reflecting the strong anti-bonding σ^* character whereas the T_2-down is non-bonding or weakly anti-bonding.

Figures 1(a) and (b) schematically illustrate the p-DOS from figure 2 without and with the inclusion of the d orbitals. The levels are broadened by a Gaussian to mimic the 'banding' effects in an extended material. The energy separation of these levels is calculated with EHMO to be about 33 eV for an Al–O bond length of 1.70 Å. Performing full [9] and real-space [1] multiple scattering calculations on a single-shell cluster gives two peaks in the near-edge region. The T_2-up in this case is positioned at about 20 eV above the Fermi level. This is in good agreement with the experiment. The discrepancy between the experiment and the EHMO calculation can be ascribed to the limitations of the EHMO method and partly because of the unrealistically highly charged clusters that have to be used as discussed in section 2. It is stressed here that the EHMO results, as mentioned above, are not quantitative; nonetheless, they show the proper trends [24].

In order to investigate the bonding/anti-bonding nature of these two T_2-levels, the change in energy as a function of varying Al–O bond length is analysed and shown in figure 3. Results are shown from the full multiple scattering and the EHMO calculations. For ease of comparison, all energies are set equal to zero at 1.70 Å. In this way the results from both the calculations are compared on a relative scale. The T_2-up level is strongly shifted towards higher energy with shorter Al–O bond length in both the calculations. This behaviour reveals the strong anti-bonding character of this energy level.

The T_2-up peak is fairly well reproduced in a multiple scattering calculation with a single-shell calculation [1, 9]. Further, including higher shells does not significantly alter this peak. Hence, this peak has a predominantly localized character. Combining this with the sensitivity towards Al–O bond length, this peak is assigned to a local Al–O anti-bonding σ^* orbital. In contrast, the energy position of the T_2-down is nearly unaffected by the changes in the Al–O bond length (figure 3) and can therefore be assigned as non-bonding, or weakly anti-bonding; but as will be discussed in more detail later, it has a much more radially extended character.

The observed splitting of the d orbitals for aluminium is large in comparison with the splitting generally observed for transition metals. The reason for this is the contracted nature of the d orbitals in the transition metals, whereas in aluminium the d orbitals have a more diffuse character. This diffuse character results in a larger overlap with the orbitals of the neighbouring atoms increasing the 'crystal field' splitting.

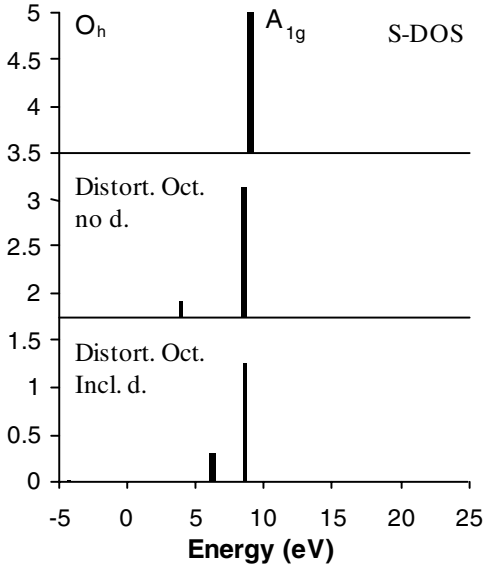

Figure 4. The s orbital DOS as calculated by EHMO on an $Al^{\subseteq}O_6^{8-}$ cluster with Al in O_h symmetry without the inclusion of d orbitals (top), in a distorted octahedral cluster, without the inclusion of d orbitals (middle) and with the inclusion of d orbitals (bottom) showing the splitting of the s DOS due to geometric distortions and some s–d hybridization.

3.3. Orbital hybridization in octahedral Al

While p–d hybridization in tetrahedral coordination is very significant, it is not allowed in octahedral coordination due to reasons of symmetry. This is verified by the EHMO calculations on an octahedrally coordinated aluminium, which do not show any effects on the calculated p-DOS (or s-DOS) after incorporating the d orbitals. However, if the octahedron becomes distorted (figure 4), hybridization of p (and s) with the d orbitals is allowed and the p-DOS (and s-DOS) will change accordingly. Indeed, any geometrical distortion causes the p (and s) orbitals themselves to split. In figures 4–6, these influences of distortions on the unoccupied s, p and d orbitals, respectively, are shown in the results of the EHMO calculations on $Al^{\subseteq}O_6^{-8}$ clusters. In each of these figures, the top section represents the DOS calculated on a perfect octahedron (Al–O = 1.91 Å) and the middle and bottom on a distorted octahedron without and with the inclusion of the d orbitals, respectively. The octahedral is distorted as in corundum. The distorted octahedral in corundum is used in the literature as a reference compound for octahedral Al [6, 9, 25], which is therefore a logical choice to take as a reference here. Aluminium in corundum has two different Al–O distances: three $Al–O_a = 1.86$ Å and three $Al–O_b = 1.97$ Å and the O–Al–O angles are distorted from 90°: three $O_a–Al–O_a = 86.4°$, three $O_b–Al–O_b = 101.1°$ and six $O_a–Al–O_b = 79.9°$ [26].

A perfect octahedron shows just one A_{1g} s-level in figure 4, whose energy is very sensitive to the Al–O bond length. Distorting the octahedron (figure 4, middle plot) results in a loss of symmetry and accordingly, the A_{1g} splits into several different levels. Hybridization with the d orbitals (figure 4, bottom plot) is allowed and an additional level with small intensity appears at very low energy. The behaviour of the p-DOS (figure 5) as a function of distortion and the presence of the d orbitals is very similar to that of s-DOS. As expected, the p-DOS (figure 5) results in a single T_{1u} level whose energy is also Al–O bond length-sensitive for a perfect octahedron. Geometric distortions (figure 5, middle plot) indicate that the T_{1u} level is split into

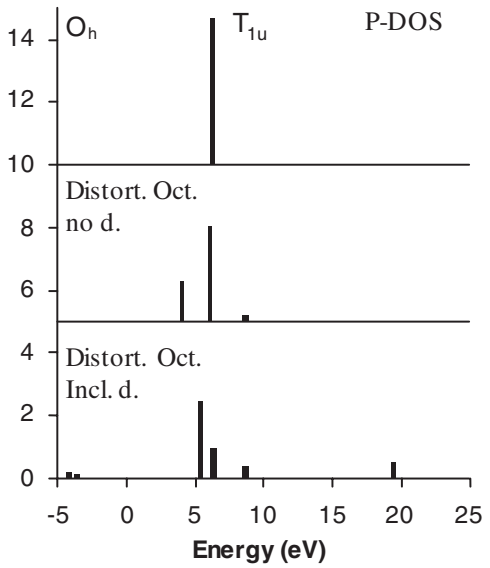

Figure 5. Same as in figure 4 but for the p orbital DOS.

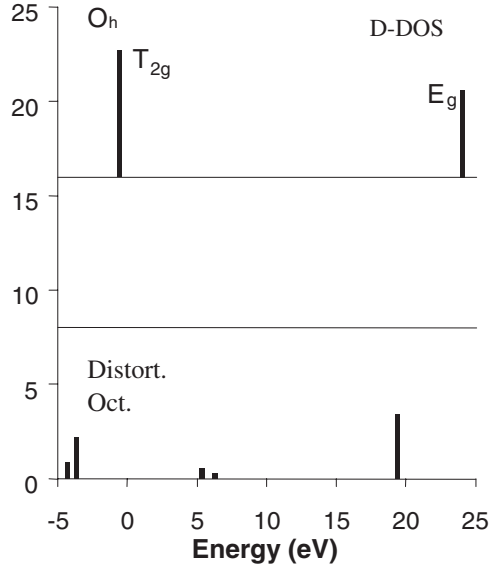

Figure 6. Same as in figure 4 but for the d orbital DOS.

several levels and comparison with figure 4 shows that some s–p hybridization has occurred. In this case, d orbital hybridization produces a large effect (figure 5, bottom plot) with the p-DOS spread over a wide energy range. The splitting of the d orbitals in an O_h environment gives the usual T_{2g} and E_{2g} splitting (figure 6). When the octahedron is distorted, a shift to lower energy occurs and some additional states with small d orbital components appear.

In summary, upon distortion of the octahedron, the s- and p-DOS are spread over more energy levels arising solely due to symmetry breaking or geometrical effects. The p orbitals can now hybridize strongly with the d orbitals producing further large changes, whereas the s–d hybridization effects are much smaller.

It must be emphasized here that the XANES experimental spectra cannot be interpreted by calculations on just one-shell clusters due to the long-range effects as mentioned in the previous paragraph (this is especially true at the K-edge). This will be dealt with extensively in the next section. However, these calculations reveal the importance of the p–d hybridization in the determination of the spectral lineshapes. Moreover, these calculations prove that the XAS spectra of distorted structures cannot simply be assigned on the basis of calculations performed on non-distorted clusters.

3.4. Long-range effects

It is reported that the $L_{II/III}$ spectra of low Z elements consist of localized quasi-molecular 'inner well resonances'. Below the continuum threshold, discrete inner well states called 'core excitons' also appear [27]. Both the localized resonances and the excitons should be well reproduced in the calculations with just a single shell of atoms about the absorber atom. However, as mentioned previously [1, 9], a full multiple scattering calculation on a cluster with a single shell about an Al absorber atom is not able to reproduce the fine structure in the region 0–15 eV above the threshold at the K-edge. In order to reproduce the fine structure in the Al XANES in either octahedral or tetrahedral coordination, at a minimum, a medium-range ordering ($\sim$15 Å) is taken into account [9]. When calculations on the clusters with diameters

up to 15 Å were performed, all the fine structure was reasonably well reproduced. Our FEFF8 results fully reproduce this as clusters containing further than next nearest neighbours are necessary to reproduce the fine structure (figure 8(b)). This is also confirmed by the experimental $L_{II/III}$-edge spectra for octahedral Al present in a single monolayer of Al_2O_3. These data show much broader peaks in the 0–15 eV region compared to the bulk Al_2O_3 [27].

Although medium-range multiple scattering appears to be important at both the $L_{II/III}$- and K-edges of Al, a more specific conclusion is obtained for the Si edges [24]. A comparison of the spectra at the Si K- and $L_{II/III}$-edges on gaseous and solid-state silicon compounds revealed that the $L_{II/III}$-edges are dominated by shape resonances, whereas at the K-edge multiple scattering over a long range must be taken into account in order to assign the spectra properly. For the $L_{II/III}$-edge, both the spectra of gaseous and solid-state compounds were well reproduced by the theoretical MO calculations, whereas at the K-edges, the solid-state spectra contained additional peaks due to multiple scattering or extended band structures [24]. The same study showed that iso-electronic structures display very similar features in their absorption spectra and these features have identical origins. Thus, we assume that long-range multiple scattering is even more important at the K-edge than at the $L_{II/III}$-edge for Al, although it is not negligible at either edge.

In figure 1(c) the effect of long-range ordering on the spectra is shown schematically by the fine structure appearing in the region 0–15 eV above the absorption edge. This is in sharp contrast to the σ^* anti-bonding peak, appearing at $\sim$20 eV above the edge, which is already well reproduced in a single-shell calculation and hence is relatively unaffected by multiple scattering beyond the first shell. However, multiple scattering in the first shell is required to determine the shape and position of the σ^* peak, since as an antibonding resonance, it is reproduced in a scattered-wave calculation by high-order multiple scattering between the two atoms involved in the bond [28].

The origin of long-range scattering can be attributed to the diffuse molecular orbitals participating in the bonding in this energy region. As discussed in the previous section, due to hybridization of the d orbitals, the diffuse character of the d orbitals is hybridized with the s and p orbitals (figures 4–6) that are probed in the $L_{II/III}$- and K-edge spectra, respectively. An overlap of MOs with the next nearest neighbour Al (or Si) atoms results in a near edge that is determined by medium-range ordering (up to 15 Å). For the $L_{II/III}$-edge spectra, these multiple scattering features are much smaller in magnitude, since the d orbitals hybridize much less with the s orbitals, so that the s orbital density sampled at the $L_{II/III}$-edge is more local [24].

3.5. Core hole–photoelectron attraction

Having established the importance of distortions and hybridization of the d orbitals on the shape of the spectra, the effect of the core hole–photoelectron attraction is now discussed.

While the intensity of an electronic transition is determined by the initial state, the shape of the probed DOS is determined by the final state. In an XAS experiment, a core hole is created, while the photoelectron (at least in the near-edge region) is excited into empty valence states. The core hole contributes a positive charge, which has a mutual attraction with the negatively charged photoelectron. The effective energy of the transition in the XAS therefore is $h\nu = \Delta E - \boldsymbol{U}$, where ΔE is the energy difference between the initial-state energy level and the target final-state energy level. Here $\boldsymbol{U}$ is the core hole–photoelectron attraction [29]. The size of $\boldsymbol{U}$ is determined by two factors: (i) the direct attraction between the core hole and the photoelectron, which is determined by the radial extent of the final-state valence orbital, and (ii) the amount of screening of the core hole by valence electrons, which have moved closer to the core hole in response to the increased Coulomb force. A fully screened core hole

causes $\boldsymbol{U}$ to decrease to near zero. The effect of the core hole attraction on the DOS is shown schematically in figure 1(d). Here, the conduction band spectral density is deformed towards lower energies. The appropriate mathematical expression for describing this deformation is given by Economou [29]. The DOS calculations using FEFF8 show the influence of the core hole on the shape of the p-DOS [5]. The magnitude of the deformation is highly determined by the size of $\boldsymbol{U}$ and thus on the amount of screening. A very large $\boldsymbol{U}$ causes energy levels to become separated from the conduction band at the edge and hence gives rise to a true exciton. The factors that determine the extent of this screening are dealt with in the next section.

4. Discussion

4.1. Edge position of octahedral and tetrahedral Al: hybridization, mixing and screening

It is well known from the literature [1–10] that the edge position in the Al XANES spectra of tetrahedral Al is about 2 eV lower than that for octahedral Al. It is proposed that the edge position in five-coordinated Al is positioned in between the four- and six-coordinated Al [1]. In spectra of distorted octahedral Al, a pre-edge feature is visible that aligns with the edge of the tetrahedral aluminium. These differences in XAS spectra are used to distinguish tetrahedral- from octahedral-coordinated Al. In fact, many papers have been published on this topic.

Based on our calculations, there are two reasons why the edge position of the tetrahedral Al is positioned at a lower energy than that for octahedral Al, both involving the symmetry. Both are illustrated in figure 7, which is a schematic illustration of figures 2, 4–6 and the energy diagram for metals in T_d coordination [30]. The solid lines indicate the initial-state levels and the dashed lines indicate the levels adjusted for the core hole (final state). Figure 7(a) reveals the p–d hybridization in T_d symmetry. The anti-bonding and non- or weakly bonding character of the T_2-up and T_2-down, respectively, is indicated. Moreover, the anti-bonding character of the A_{1g} is revealed. All these levels have an overlap with the adapted symmetry orbitals on the oxygen atoms of appropriate symmetry. A non-bonding highest occupied molecular orbital (HOMO) T_1 level on the oxygen atoms is shown, which has the wrong symmetry to mix with any of the Al lowest unoccupied molecular orbitals (LUMOs). The dashed line reveals the T_2-down level after the creation of the core hole, with core hole attraction, $\boldsymbol{U}$ is indicated. The position of this peak determines the energy of the edge for tetrahedral Al at the K-edge. Thus two factors determine the energy of T_2-down: (i) the p–d hybridization pushing it down and (ii) the core hole attraction $\boldsymbol{U}$ pushing it even further down.

Figure 7(b) reveals the overlap of the Al levels with the symmetry-adapted oxygen levels in an O_h conformation as obtained from figures 2, 4–6 and the energy diagram for the metals in the O_h coordination [30]. No p–d or s–d hybridization is allowed. However, a HOMO T_{1u} non-bonding symmetry-adapted orbital on the oxygen has the same symmetry as the LUMO T_{1u} on the Al, allowing mixing of these two orbitals upon the introduction of the core hole. These orbitals are allowed to mix because the potential on the absorber atom has changed; however, the symmetry has not changed. Therefore, only orbitals of the same symmetry can mix. This is highlighted in figure 7(c) where only the orbitals with T_{1u} symmetry within the marked box in figure 7(b) are given. The solid lines indicate that the T_{1u} on Al overlaps with the T_{1u} on oxygen. However, upon the creation of the core hole, the T_{1u} on Al experiences a large core hole shift, $\boldsymbol{U}$, due to the primarily Al p character of this orbital. This is indicated by the slashed line. This lowering of the T_{1u} level increases the overlap with the T_{1u} on oxygen, pushing it back up again. Moreover, the filled bonding orbital now contains more Al character, which is viewed as electron transfer from oxygen to aluminium, to help screen the

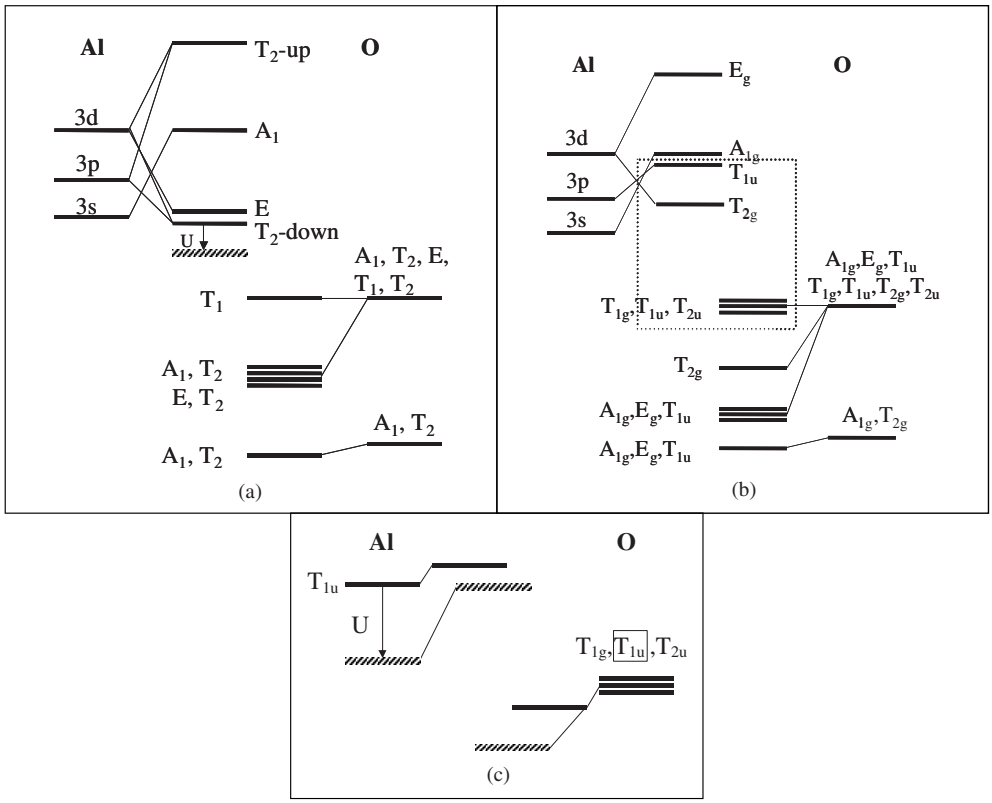

Figure 7. (a) Schematic MO diagram for tetrahedral AlO_4. p–d hybridization is shown. Here ***U*** identifies the core hole attraction in the XAS final state, which lowers the 'T_2-down' level as shown by the dashed line. (b) Schematic MO diagram for octahedral AlO_6. No p–d hybridization is allowed in this symmetry. The orbitals with T_{1u} symmetry in the marked box are redrawn in (c). (c) Schematic showing of the T_{1u} level mostly on the aluminium (the LUMO) interacting with the non-bonding T_{1u} (HOMO) on oxygen. In the presence of the core hole, the Al T_{1u} levels get pulled down (U), increasing the covalent interaction with the oxygen-T_{1u} and hence it is pushed back up. By this interaction, electron density on oxygen is transferred to Al, whereby the core hole in octahedral Al is screened.

core hole. Hence, in octahedral Al, the edge energy is determined by the mixing of T_{1u} with a symmetry-adapted T_{1u} orbital on oxygen, facilitating charge transfer from oxygen to Al and increasing the screening of the core hole.

This mixing of the oxygen p with the Al p shows that in the octahedral case some cationic character is present at the VBM, whereas the VBM DOS in tetrahedral Al is completely anionic, as was put forward by Cabaret *et al* [9]. The different orbital symmetry in tetrahedral versus octahedral Al dictates this difference.

In conclusion, the edge position of tetrahedral Al is positioned at lower energy because of p–d hybridization, which only occurs in the T_d symmetry (T_2-down in figure 7(a)). A second reason concerns the screening. In O_h symmetry, the core hole is screened by a charge transfer from oxygen to Al, that is, symmetry forbidden in T_d. Therefore, in order to reproduce the XAS spectra of tetrahedral Al, an unscreened potential must be used, whereas in octahedral symmetry the core hole is more screened and as a consequence a more shielded potential must be used. This is further verified by a comparison of the FEFF8-calculated Al atom charges in

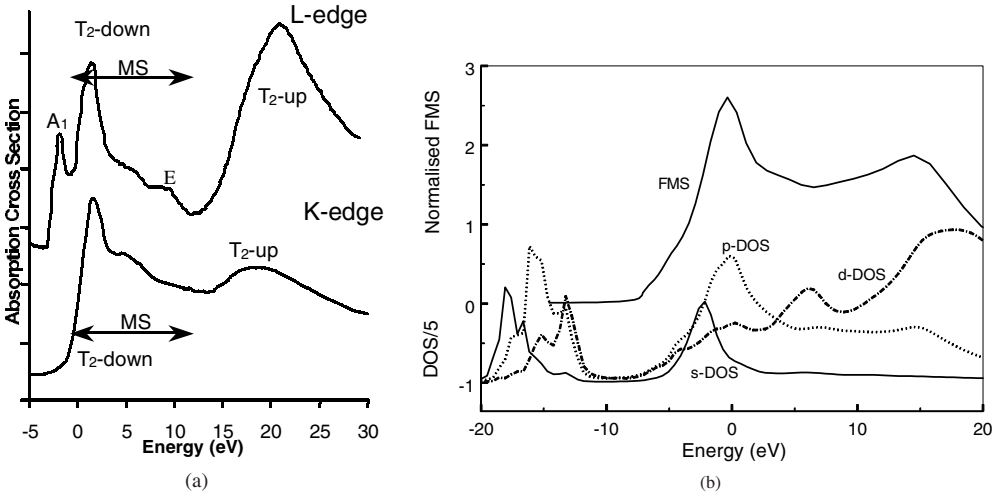

Figure 8. (a) Experimental Al $L_{II/III}$ (top) and K (bottom) edge XANES spectra for tetrahedral aluminium. An assignment of the spectra is indicated. Here, the features attributed to T_2-up and T_2-down are labelled and the arrows mark the region that is determined by long-range multiple scattering as discussed in the text. The $L_{II/III}$-edge contains a pre-edge feature that is assigned to the A_1 orbital having a primarily s character, but also contains p and d characters (see text for more details). (b) SFC FMS calculations using FEFF8 on a $AlSi_{29}O_{74}(H)$ cluster representing zeolite beta, containing tetrahedral Al. The XAS (top) and the s-, p- and d-DOS (bottom) are given.

the presence of a core hole ($O_h = +0.572$ versus $T_d = +0.737$). The smaller plus charge in the O_h case reveals the O charge transfer to screen the core hole.

A small pre-edge feature is always visible in the experimental K-edge spectra of distorted octahedral Al. This pre-edge feature aligns with the tetrahedral whiteline. Even small distortions allow some s–p–d hybridization and this lowers the energy levels very similar to that in the tetrahedral case (figures 4–6 and 9(b)).

4.2. Experimental K- and L-edges of tetrahedral and octahedral Al compared to SCF-FMS and DOS calculations

In figures 8 and 9, experimental and theoretical XAS spectra at the $L_{II/III}$- and K-edges and calculated DOS for tetrahedral (figure 8(a) and (b)) and octahedral Al (figure 9) are compared. Assuming the $\Delta l = \pm 1$ selection rule is valid, the p-DOS is sampled at the K-edge, and the s- and d-DOS at the $L_{II/III}$-edge. The calculated p-DOS clearly has a similar shape to the K-edge spectra for tetrahedral aluminium. The shape of the d-DOS is very similar to the experimental $L_{II/III}$-edge spectra, except for the dominant pre-edge features in the $L_{II/III}$-edge that primarily contain s-DOS. It also appears that the s-DOS is very small compared to the d (except for the pre-edge features), so that all the peaks in the $L_{II/III}$-edge spectrum can be assigned based on the d-DOS.

The similarity between the $L_{II/III}$- and K-edges for both tetrahedral and octahedral Al is evident. Many peaks appear at the same energy position; however, the intensities vary greatly. This section will discuss these spectra based on the results obtained in the previous paragraphs and the DOS calculations. The XAS peaks generally arise from mixed states; nonetheless the assignment we give is generally based on the symmetry of the orbital with the dominant content.

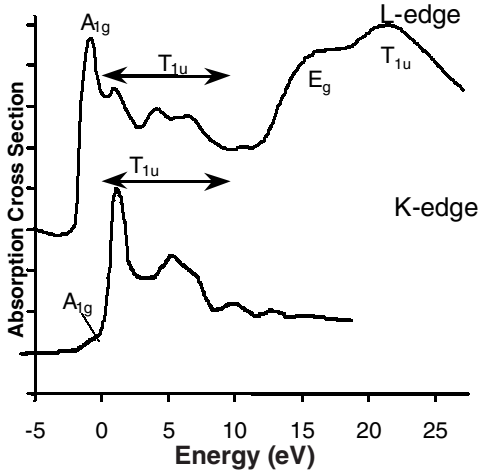

Figure 9. Experimental Al $L_{II/III}$ (top) and K (bottom) edge spectra for octahedral aluminium (corundum). A proposed assignment of the spectra is indicated. Arrows mark the regions that are determined by long-range multiple scattering in both the edges.

4.3. Tetrahedral Al

The FEFF8 results for the largest $AlSi_{29}O_{74}$ cluster representing zeolite beta are given in figure 8(b), including the XAS and the relevant DOS. Both the experimental spectra show a sharp whiteline that is preceded in the $L_{II/III}$-edge spectrum by a large distinct pre-edge feature. In the region 5–15 eV above the edge in both spectra, a fine structure is visible. Finally, at higher energies ($\sim$20 eV) both the edges show a broad feature, which extends to a higher energy in the $L_{II/III}$-edge spectrum.

The pre-edge peak in the $L_{II/III}$-edge spectrum is often attributed to the A_1 level [7]. This is confirmed by the FEFF8 DOS showing a clear peak with the s character just below the first maximum in the p-DOS. A small amount of p and d density is present at this low energy; however, no clear pre-edge peak is observed in the K-edge spectra.

The T_2-down levels (figure 8(a)) are primarily responsible for the intensity and the fine structure above the absorption edge (at energies $< \sim$15 eV) in both the K [1]- and $L_{II/III}$ [27]-edge experimental spectra. As shown in figure 2, the T_2-down resonance contains both p and d characters, which produces the intensity in the K- and $L_{II/III}$-edges, respectively. The FEFF8 calculations indicate that the fine structure just above the absorption edge only appears in the calculations on clusters with sizes larger than $\sim$12 Å. Calculations on small clusters give results essentially identical to previously published results on small clusters [5, 9], which also show no fine structure at 0–15 eV above the edge.

The small feature around $\sim$11 eV, visible in the $L_{II/III}$-edge is reproduced by a peak in the d-DOS. A small feature appears at $\sim$11 eV already in the spectra of small gaseous molecules, such as $Si(CH_3)_4$, where long-range multiple scattering is not possible; in this case it was attributed to the E level [24]. Although the s- and p-DOS also show a very small feature around 11 eV, only a very small inflection in the K-edge spectrum is visible at this energy.

The peaks at 20 eV and higher in both the K- and $L_{II/III}$-edges are determined by the mixed p–d T_2-up orbital. As shown in the calculated d-DOS, the peak at $\sim$20 eV is extended to higher energy than that for the p-DOS, which is reflected in the experimental data by a much broader peak in the experimental spectra.

4.4. Octahedral Al

In the octahedral Al case (figure 9), the dominating sharp whiteline in the $L_{II/III}$-edge spectrum [27] is visible as a small pre-edge feature in the K-edge spectrum [6]. These peaks are assigned to an s–p–d hybridized orbital giving it a non-local character because of the large diffuse d orbital component. The p character is visible in the K-edge and the s and d characters in the $L_{II/III}$-edge spectrum. This hybridization is allowed due to the distortions in the octahedron as is seen by the EHMO calculations in figure 4. It has been stressed by Cabaret that a small pre-edge feature in the calculated K-edge spectra for distorted octahedral Al is visible only for multiple scattering calculations on large clusters (∼14 Å). This is consistent with the assignment of the pre-edge feature to a diffuse hybridized s–p–d state instead of a relatively localized s state [7]. We assign the pre-edge peak to A_{1g} symmetry consistent with the large s character. The s–p–d hybridization helps to push this level to lower energy.

The whiteline and the region above (0–15 eV) the K-edge spectrum contains a fine structure that is also visible in the $L_{II/III}$ spectrum. This intensity is assigned to the diffuse p–d mixed T_{1u} orbital (figure 5); diffuse because of the d-content of this orbital.

The large doublet peak between 15 and 25 eV in the $L_{II/III}$-edge of octahedral Al is completely assigned to d-DOS. The d–p hybridization places some p character in the E_g orbital so that some intensity is expected at this energy (∼15–25 eV) in the K-edge spectrum. The E_g peak originates from the crystal field splitting of the d orbitals and is pushed up in energy in an octahedral symmetry.

5. Conclusions

MO and FEFF8 multiple scattering calculations provide good insight into the phenomena relevant to XAS spectra at the Al K- and $L_{II/III}$-edges. Most of the features can be assigned to shape resonances, i.e. short-range multiple scattering involving the first O shell. Based on this, an assignment of the major peaks in the $L_{II/III}$- and K-edge spectra is given. However, the fine structure in the region 0–15 eV arises from long-range multiple scattering.

The differences in the spectra for tetrahedral and octahedral Al can be understood based on the (s–)p–d hybridization, which is allowed in the tetrahedral case. It is shown that the d orbitals play a predominant role in the determination of the final shape of the XAS spectra at both the $L_{II/III}$- and K-edges. The diffuse d orbitals result in a near edge that is determined by long-range (up to ∼15 Å) ordering. This is true for both $L_{II/III}$- and K-edges; however, the K-edge is more sensitive to scattering over an extended area than the $L_{II/III}$-edges, primarily because the p–d hybridization is more important than the s–d hybridization. Moreover, it is shown that hybridization of the diffuse d orbitals and subsequent differences in screening of the core hole affect the position of the whitelines in the K- and $L_{II/III}$-edge spectra.

Mixing of the HOMO and LUMO on the oxygen and aluminium, respectively, allows for screening of the octahedral Al, which is not allowed in the tetrahedral case. Thus simple symmetry considerations explain why a screened core hole for the octahedral case and an unscreened core hole in the tetrahedral case need to be taken into account.

Finally, it is shown that the MO calculations on the octahedral O_h structures cannot be used to assign the spectra of *distorted* octahedron Al. Such small distortions immediately allow p–d hybridization, which significantly affects the energy and degeneracy of the orbital levels.

References

[1] van Bokhoven J A, Sambe H, Ramaker D E and Koningsberger D C 1999 *J. Phys. Chem. B* **103–36** 7557
[2] Landron C, Badets M C, Douy A, Coutures J, Coutures J P, Daniel P and Flank A M 1991 *Phys. Status Solidi* **167** 429
[3] Wyckoff R W G 1963 *Crystal Structure* vol 1 2nd edn (New York: Wiley)
[4] Ildefonse Ph, Kirkpatrick R J, Montez B, Cala G, Flank A M and Lagarde P 1994 *Clays and Clay Minerals* **42** 276
[5] van Bokhoven J A, Sambe H, Koningsberger D C and Ramaker D E 1997 *J. Phys. IV France* 1997 **7** Colloque C2, Supplément au Journal de Physique III d'Avril C2-835
[6] McKeown D A, Waychunas G A and Brown Jr G E 1985 *J. Non-Cryst. Solids* **74** 349
[7] Li D, Bancroft G M, Fleet M E, Feng X H and Pan Y 1995 *Am. Mineral* **80** 432
[8] Waychunas G A and Brown Jr G E 1984 *EXAFS and Near Edge Structures III* ed K A Hodgts, B Hedman and J E Penner-Hahn (Berlin: Springer) p 336
[9] Cabaret D, Sainctavit P, Ildefonse Ph and Flank A-M 1996 *J. Phys.: Condens. Matter* **8** 3691
[10] Bugaev L A, Ildefonse Ph, Flank A M, Sokolenko A P and Dimitrienko H V 1998 *J. Phys.: Condens. Matter* **10** 5463
[11] Tossell J A 1975 *J. Am. Chem. Soc.* **97** 4840
Tossel J A 1975 *Chem. Solids* **36** 1273
Tossell J A 1973 *Geochimica et Cosmochimica Acta* **37** 583
[12] van Bokhoven J A, Sambe H, Ramaker D E and Koningsberger D C 1999 *Proc. XAFS X Conf. (Chicago), J. Synchr. Rad.* **6** 207
[13] van Bokhoven J A, Ramaker D E and Koningsberger D C *J. Phys.: Condens. Matter* submitted
[14] Natoli C R, Misemer D K, Doniach S and Kutzler F W 1995 *J. Phys.: Condens. Matter* **7** 2353
[15] Schober H and Dorner B 1994 *J. Phys.: Condens. Matter* **6** 5351
[16] Kefi M, Jonaard P, Evergand F, Bonelle C and Gillet E 1993 *J. Phys.: Condens. Matter* **5** 8629
Ching W Y and Xu Y-N 1994 *J. Am. Ceram. Soc.* **77** 404
[17] van der Erden A, van Bokhoven J, Smith A and Koningsberger D 2000 *Rev. Sci. Instrum.* **Vol 71-9** 3260–3266
[18] Howell J, Quantum Chemistry Program Exchange #344 Indiana University, Bloomington, contained in Hyperchem O, Hypercube, Inc. Waterloo, Ontario N2L3X2, Canada
[19] Burns G 1964 *J. Chem. Phys.* **41** 1521
[20] Schwarz W H E 1976 *Chem. Phys.* **13** 363
[21] Ankudinov A L, Ravel B, Rehr J J and Conradson S D 1998 *Phys. Rev.* B **58** 7565
[22] Mustre de Leon J, Rehr J J, Zabinski S I and Albers R C 1991 *Phys. Rev.* B **44** 4146
[23] Rehr J J 1993 *J. Appl. Phys.* **32** 8
[24] Sutherland D G J, Kasrai M, Bancroft G M, Liu Z F and Tan K H 1993 *Phys. Rev.* B **48** 14989
[25] Mottana A, Robert J-L, Mercelli A, Giouli G, Della Ventura G, Paris E and Wu 1997 *Z. Am. Mineral* **82** 497
[26] Newnham R E and De Haan Y M 1962 *Z. Kristallogr.* **117** 235
[27] Bianconi A 1979 *Surf. Sci.* **89** 41
[28] Rehr J J, Albers R C and Zabinsky S I 1992 *Phys. Rev. Lett.* **69** 3397
[29] Economou E N 1979 *Green's Functions in Quantum Physics (Springer Series in Solid-State Sciences vol 7)* (Berlin: Springer)
[30] Cotton F A 1990 *Chemical Applications of Group Theory* 3rd edn (New York: Wiley)